VSP J. Adhesion Sci. Technol. (2011) DOI:10.1163/156856111X599599

Journal of ADHESION SCIENCE and TECHNOLOGY
brill.nl/jast

Endcapping Treatment of Inner Surfaces of a Hexagonal Mesoporous Silica

Weiyi Lu [a], **Aijie Han** [b], **Taewan Kim** [c], **Brian J. Chow** [a] **and Yu Qiao** [a,*]

[a] Department of Structural Engineering, University of California — San Diego, La Jolla, CA 92093-0085, USA

[b] Department of Chemistry, University of Texas — Pan American, Edinburg, TX 78539, USA

[c] Program of Materials Science & Engineering, University of California — San Diego, La Jolla, CA 92093, USA

Abstract

The inner surfaces of a hexagonal mesoporous silica (HMS) are treated by chlorotrimethylsilane, either directly or through vapor or liquid endcapping. The directly treated inner surfaces have the highest effective interfacial tension, and the liquid endcapping treated surfaces have the largest accessible nanopore volume. The difference in the treatment results may be attributed to the distinct surface structures.

Keywords

Endcapping, inner surfaces, nanopores, HMS

1. Introduction

Nanoporous materials have been widely used by chemists and chemical engineers for catalysis, absorption and adsorption, purification, etc. [1]. Recently, their applications were extended to mechanical engineering areas. For instance, it was discovered that the infiltration of liquids in nanopores can be highly energy dissipating and/or can be controlled electrically [2], which has received increasing attention for protection and damping applications, such as bumpers, armors, helmets, as well as for electrowetting study [3].

The high performance comes from the large specific surface area. As a liquid flows in a channel, the internal friction can lead to a certain degree of energy absorption [4]. However, this effect is limited by the significant decrease in effective viscosity of confined liquid in nanopores [5, 6]. Much higher energy absorption efficiency can be achieved if the nanopore surfaces are lyophobic. To force liquid into such nanopores, the capillary effect must be overcome. As the nanopore in-

* To whom correspondence should be addressed. E-mail: yqiao@ucsd.edu

 DOI:10.1163/156856111X599599

ner surfaces are in contact with the confined liquid, the system free energy rises by $U = \gamma \cdot A$, where γ is the effective excess interfacial tension and A is the total surface area. At a nonwettable surface, the energy increase associated with the formation of a solid–liquid interface is typically on the order of 10–100 mJ/m^2 [7]. If in a nanopore the value of γ is similar to its bulk counterpart, with the large A around 10^3 m^2/g, U can be 10–100 J/g, much higher than that of many ordinary protection materials [8, 9]. Moreover, the effective solid–liquid interfacial tension in nanopores is electrically controllable, somewhat similar but different from the conventional electrowetting effect [10]. As a potential difference is applied across the interface, the system performance can be adjusted in a broad range [11].

A key process for producing electrically-controlled nanoporous energy absorption systems is the treatment of inner surfaces. Many nanoporous materials, such as nanoporous silica, are intrinsically hydrophilic. In order to activate the interfacial tension based and electrically controlled energy dissipation, the nanopore surfaces must be coated by hydrophobic layers [12–14]. Different from the surface treatment of large solid surfaces, to treat nanopore walls, many unique issues, such as the accessibility and the removal of byproducts, must be taken into consideration. While intensive study has been carried out in this field, the experimental data are still far from being complete.

In this paper, we report investigation results on the endcapping effects on hexagonal mesoporous silica (HMS) samples, which is a preliminary investigation for the future electrowetting study. Endcapping is a commonly used technique to control surface structures [15]. However, its influence on the infiltration pressure and volume, particularly for energy absorption applications, has not been systematically analyzed.

2. Experimental

The HMS sample was obtained from Sigma-Aldrich. Through a gas adsorption analysis using a Micromeritics ASAP-2020 Analyzer, the average nanopore size was measured as 6.1 nm; the nanopore volume was 0.55 cm^3/g; and the Brunauer–Emmett–Teller (BET) surface area was 630 m^2/g. The material was treated by three different methods: (1) direct treatment, (2) liquid endcapping and (3) vapor endcapping.

In the first method, the HMS sample was vacuum dehydrated at 120°C for 12 h, and then refluxed in a 2.5% dry toluene solution of chlorotrimethylsilane at 90°C for 24 h, after which the treated HMS particles were thoroughly rinsed successively with dry toluene and methanol.

In the second and the third methods, the vacuum dehydrated HMS particles were refluxed in 5% dry toluene solution of chlorodimethyloctylsilane at 90°C for 24 h. After thorough rinsing successively with dry toluene and methanol, endcapping treatment was performed. In the second method, the HMS particles were mixed in 2.5% dry toluene solution of chlorotrimethylsilane and the mixture was refluxed

at 90°C for 12 h. In the third method, the HMS particles were exposed to the vapor of chlorotrimethylsilane for 12 h. The vapor was generated by heating liquid chlorotrimethylsilane at its boiling temperature.

The treated material was immersed in saturated aqueous solution of lithium chloride (LiCl) and sealed in a stainless steel cylinder. By using a type 5580 Instron machine, a stainless steel piston was compressed into the cylinder, with a loading rate of 1 mm/min. Depending on the infiltration pressure, as will be discussed below, when the pressure reached 14 or 24 MPa, the piston was moved back to its initial position at a rate of −1 mm/min. The quasi-hydrostatic pressure was calculated as the piston force divided by the piston area (286 mm^2). The system volume reduction was assessed as the piston displacement multiplied by the piston area. After the first cycle, similar loading-unloading cycles were repeated for a few times. Typical test results are shown in Figs 1 and 2. Since no significant changes in sorption isotherm curves were detected from the 2nd cycle, the following discussion will be focused on the first two loadings.

3. Results and Discussion

From Figs 1 and 2, it can be seen that in all the cases, the sorption isotherm curves are highly hysteretic after the first loading; that is, the systems can work continuously under cyclic loadings, which is critical to electrically controlled energy

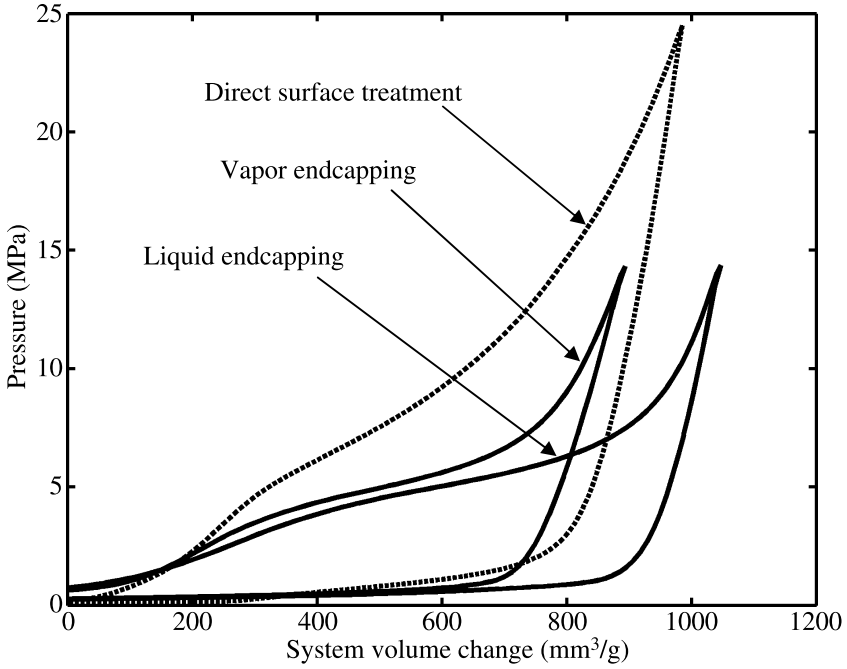

Figure 1. Typical sorption isotherm curves at the first loading.

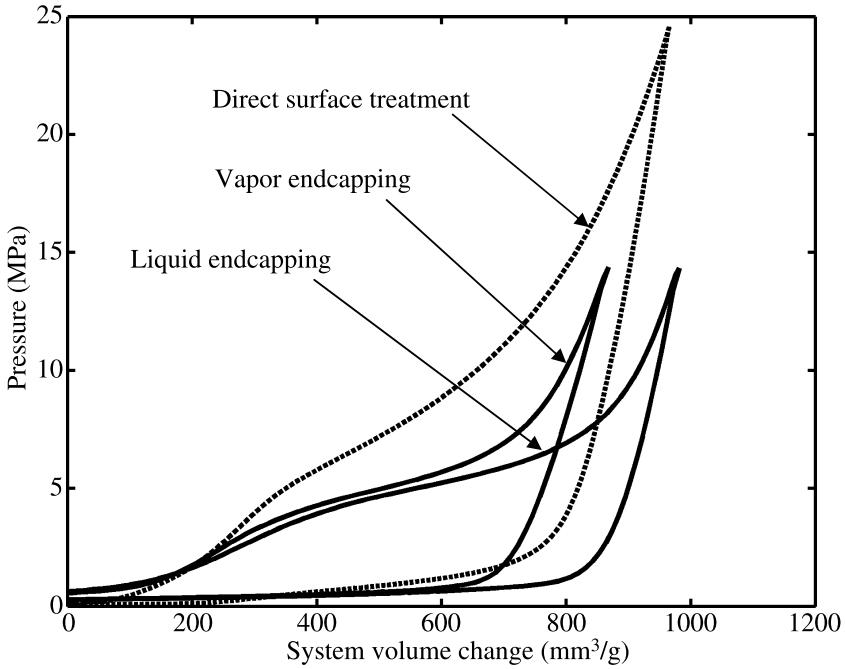

Figure 2. Typical sorption isotherm curves at the second loading.

absorption applications where multiple adjustments of potential difference are necessary.

After the surface treatment, the nanopore inner surfaces are coated with a monolayer of hydrophobic silyl groups, which can keep the liquid phase out of the nanopores under ambient pressure. The energy absorption mechanism cannot be activated when the pressure is relatively low, due to the capillary effect. When the pressure is sufficiently high, the slope of the sorption isotherm curve abruptly decreases, associated with the pressure induced infiltration. With a relatively small pressure increment, a relatively large amount of liquid can be forced into the HMS particles, and, thus, the system volume decreases rapidly. The infiltration ends when the nanopores of the HMS phase are fully occupied, after which the system compressibility decreases. When the pressure is lowered, the confined liquid does not defiltrate immediately. Liquid defiltration takes place when the pressure is much lower than the infiltration pressure, and completes when the pressure is fully removed. Thus, the absorbed energy, which is represented by the area enclosed by the infiltration–defiltration loop, can be estimated as the average infiltration pressure, P, multiplied by the infiltration volume, V. The system hysteresis can be related to the 'shear resistance' offered by the nanopore walls as well as the gas/vapor nanophase [16, 17], which is beyond the scope of the current study.

It is interesting that P and V are dependent on the treatment method. In the first method, the hydroxyl groups at the HMS inner surfaces directly react with

the treatment reagents, forming nonpolar silyl surface layer and resulting in a high degree of hydrophobicity. To overcome the capillary effect, the pressure must reach about 5 MPa. The infiltration begins with the relatively large nanopores. As the inner surfaces of smaller nanopores are exposed to the liquid phase, the required pressure to sustain the infiltration significantly increases.

In the second method, liquid endcapping is performed after silyl groups are grafted on the silica inner surfaces. It is well known that endcapping would deactivate the defect sites, which is compatible with the observation that the infiltration volume, i.e., the width of the infiltration plateau, is larger than that of the directly treated HMS by nearly 12%. If the defect density of a portion of a nanopore is high, the local surface can be effectively wettable. When HMS is immersed in the liquid, these parts of nanopores can be filled up spontaneously. As pressure is increased, these nanopores would not be involved in the pressure induced infiltration, resulting in a reduced infiltration volume. As the endcapping treatment removes most of the defects, the accessible nanopore volume is much larger, close to the total nanopore volume measured in the gas adsorption analysis.

At a large surface, if the defect density is reduced, the degree of hydrophobicity would increase, so that the capillary pressure becomes higher. However, Fig. 1 shows that the infiltration pressure considerably decreases, compared with that of the first method. The pressure decrease is less pronounced at the beginning stage of infiltration plateau, where the largest nanopores dominate. In the final stage of the infiltration plateau, where the liquid infiltration occurs in the smallest nanopores, the pressure difference can be a few times larger. This unique phenomenon may be attributed to the confinement effect of the nanopore walls on the liquid motion. In a large channel, the capillary pressure is determined by the solid–liquid interfacial tension. In a nanopore, in addition to the resistance caused by surface tension, the applied pressure must also overcome the 'shear resistance' offered by the solid atoms to the liquid molecules/ions in the interface layer [18]. Because in a nanoenvironment the surface to volume ratio is ultrahigh, the 'shear resistance' can be much more important than the surface tension effect. In the endcapped HMS nanopores, while the effective solid–liquid interfacial tension is somewhat higher, the 'shear resistance' may be much lower, especially in the relatively small nanopores, because of the complicated structure of their surface coating. The grafted surface groups are relatively long, and the endcapped groups are relatively short. As the rotation angle and the bond angle of surface chain vary, the boundary layer of the endcapped inner surface is more 'flexible', so that configurations of liquid molecules/ions with lower system free energies can be achieved as they move along the solid wall. The reduction in infiltration pressure may also be associated with the confined gas/vapor nanophase, for which the complicated surface features provide solvation sites.

In the third method, the endcapping is performed by the vapor phase. While vapor molecules may be more mobile than the dissolved ones in toluene, the infiltration volume is smaller than that of the second method. Clearly, less surface defects are deactivated, and, therefore, the area of the surface involved in the pressurized

liquid motion is reduced, probably due to the relatively low molecular density in the vapor phase. The infiltration volume of the so-endcapped HMS is larger than that of the directly treated one, suggesting that the endcapping treatment is still beneficial. The infiltration pressure in the third method is in between that of the first and the second methods, as it should be, as the surface structure can be somewhat regarded as a combination of the first two cases.

Figure 2 shows that at the second loading, all the characteristics discussed above remain similar, i.e., the infiltration–defiltration process is repeatable and the energy absorption system is reusable. The infiltration volumes of the endcapped HMS samples decrease slightly, and the decreases in V of the directly treated HMS is more evident.

4. Concluding Remarks

To summarize, the effects of silyl endcapping treatment on energy dissipation of liquid infiltration in an HMS sample are investigated. Endcapping would increase the accessible nanopore volume, indicating that the surface defect density is reduced. However, the infiltration pressure decreases, which may be caused by the 'shear resistance' between the nanopore wall and the confined liquid, as well as by the different behaviors of confined gas/vapor nanophase, the details of which are still under investigation. Vapor endcapping is less efficient than liquid endcapping, probably due to the lower molecular density in the vapor phase.

Acknowledgement

This work was supported by the National Science Foundation under Grant No. ECCS-1028010.

References

1. S. B. Jenkins, *Nanoporous Materials: Types, Properties, and Uses*. Nova Sci. Publ., New York (2010).
2. W. Lu, T. Kim, A. Han, X. Chen and Y. Qiao, *Langmuir* **25**, 9463–9466 (2009).
3. W. Lu, A. Han, T. Kim, V. K. Punyamurtula, X. Chen and Y. Qiao, *Appl. Phys. Lett.* **94**, 023106.1–3 (2009).
4. J. M. C. Li, *J. Alloys Compounds* **310**, 24–28 (2000).
5. A. Han, W. Lu, V. K. Punyamurtula, X. Chen, F. B. Surani, T. Kim and Y. Qiao, *J. Appl. Phys.* **104**, 124908.1–4 (2008).
6. G. X. Cao, Y. Qiao, Q. L. Zhou and X. Chen, *Molecul. Simul.* **34**, 1267–1274 (2008).
7. D. Myers, *Surfaces, Interfaces, and Colloids: Principles and Applications*. Wiley-VCH, New York (1999).
8. A. Han, V. K. Punyamurtula, T. Kim and Y. Qiao, *J. Mater. Eng. Perform.* **17**, 326–329 (2008).
9. A. Han and Y. Qiao, *J. Phys. D — Appl. Phys.* **40**, 5743–5746 (2007).
10. T. Zhang, K. Chakrabarty, R. B. Fair and S. E. Lyshevsky, *Microelectrofluidic Systems: Modeling and Simulation*. CRC Press, Boca Raton, FL (2002).

11. A. Han and Y. Qiao, *Appl. Phys. Lett.* **91**, 173123.1–3 (2007).
12. A. Han and Y. Qiao, *Chem. Lett.* **36**, 882–883 (2007).
13. A. Han and Y. Qiao, *Chem. Phys. Lett.* **454**, 294–298 (2008).
14. A. Han, V. K. Punyamurtula and Y. Qiao, *Chem. Eng. J.* **139**, 426–429 (2008).
15. M. H. Lim and A. Stein, *Chem. Mater.* **11**, 3285–3295 (1999).
16. J. Zhao, P. J. Culligan, Y. Qiao, Q. Zhou, Y. Li, M. Tak, T. Park and X. Chen, *J. Phys.: Condens. Matter* **22**, 315301.1–12 (2010).
17. L. Liu, X. Chen, W. Lu, A. Han and Y. Qiao, *Phys. Rev. Lett.* **102**, 184501.1–4 (2009).
18. Y. Qiao, L. Liu and X. Chen, *Nano Lett.* **9**, 984–988 (2009).